Article

Measurements and Simulations of the Acidity Dependence of the Kinetics of the Iron-Catalyzed Belousov−Zhabotinsky Reaction: Proton-Catalysis in the Electron Transfer Reaction Involving the [Fe(phen)₃]³⁺ Species

Ethan Zars,[†] Rainer Glaser,[*,†] Marco Downing,[†,‡] and Carmen Chicone[*,‡]

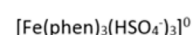[†]Department of Chemistry, University of Missouri, Columbia, Missouri 65211, United States
[‡]Department of Mathematics, University of Missouri, Columbia, Missouri 65211, United States

Ⓢ *Supporting Information*

ABSTRACT: The acidity dependence of the iron-catalyzed bromate-malonic acid Belousov−Zhabotinsky reaction was studied in the range $0.36 \text{ M} < [\text{H}_2\text{SO}_4]_0 < 1.20 \text{ M}$, and the temporal evolutions of the oscillation patterns were analyzed. The experimental results show that the period times PT_i decrease exponentially with increasing acidity and that the period times parallel the decrease of the reduction times RT with increasing acidity. Simulations using the reactions of the commonly accepted core reaction mechanism failed to match the measurements even in a qualitative fashion. However, we found that compelling agreement between the experiments and the simulations can be achieved over the entire range with the inclusion of second-order proton-catalysis of the oxidation of bromomalonic acid (BrMA) by the $[\text{Fe(phen)}_3]^{3+}$ species in the

reaction identified in this paper as reaction 9 (R9), and this $[\text{H}^+]$ dependence is informative about the species involved in the outer sphere electron transfer reaction. The trication $[\text{Fe(phen)}_3]^{3+}$ species is stabilized by ion pairing and solvation, and one may anticipate the presence of $[\text{Fe(phen)}_3(\text{HSO}_4)_n(\text{H}_2\text{O})_m]^{(3-n)+}$ species ($n = 0-3$). Our results suggest that the removal of aggregating HSO_4^- ions by protonation creates a better oxidant and facilitates the approach of the reductant BrMA, and the second-order $[\text{H}^+]$ dependence further suggests that BrMA is primarily oxidized by a doubly charged $[\text{Fe(phen)}_3(\text{HSO}_4)_1(\text{L})_k]^{2+}$ species. Considering the complexity of the BZ system and the uncertainties in the many reaction rate constants, we were somewhat surprised to find this high level of agreement by (just) the replacement of R9 by R9′. In fact, the near-quantitative agreement presents a powerful corroboration of the core reaction mechanism of the BrMA-rich BZ reaction, and the replacement of R9 by R9′ extends the validity of this core reaction mechanism to acidities above and below the typical acidity of BZ reactions ($[\text{H}^+] \approx 1$ M).
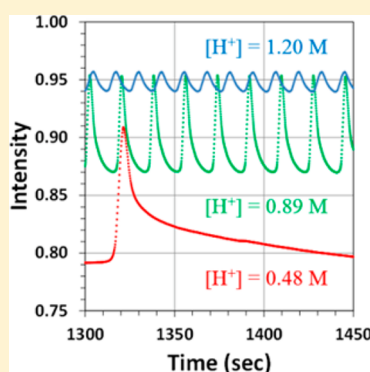
■ INTRODUCTION

The classical Belousov−Zhabotinsky (BZ) oscillating reaction refers to the oscillatory cerium-catalyzed bromate oxidation of citric acid.[1−3] Since the original discovery of the BZ reaction many similar oscillating chemical reactions have been discovered that use dicarboxylic acids (malonic acid and malic acid) as the organic substrate and are catalyzed by other metals such as Fe,[4] Ru,[5−7] Mn,[8−11] and Cu.[12] Oscillating reactions using organic molecules instead of a catalyst have also been reported.[13−18] More recent research on the BZ reaction has focused on oscillating polymer formation,[19−21] oscillating reactions inside of micelles,[19,22] communication between such micelles as a model system of neural networks,[23−26] and the complex mathematics of oscillating systems.[27,28]

Field, Köros, and Noyes (FKN) proposed the core mechanism to explain the oscillations of metal-catalyzed BZ

reactions using three processes.[29] This FKN mechanism involves (1) bromide consumption, (2) autocatalytic formation of an oxidizing intermediate ($\text{BrO}_2^{\bullet}$) and oxidation of the redox catalyst, and (3) reduction of the redox catalyst by oxidation of the organic substrate with concomitant releases of bromide back into the system. The classical FKN reactions are shown in Table 1 along with a few newer reactions and the best rate constants for each reaction.[30−37]

We wanted to test the validity of the kinetic scheme for the core mechanism of the BZ reaction against an extensive kinetic data set measured for series with varying initial conditions. Systematic variation of acidity is an obvious first choice. Smoes first studied the effects of the initial sulfuric acid concentration

Table 1. Reactions and Rate Constants for BZR Simulation

reaction	formula	rate constant	ref
R1	$HOBr + Br^- + H^+ \rightleftarrows Br_2 + H_2O$	$k_{1f} = 8 \times 10^9$	30
		$k_{1r} = 110$	
R2	$HBrO_2 + Br^- + H^+ \rightleftarrows 2HOBr$	$k_{2f} = 3.0 \times 10^6$	30
		$k_{2r} = 2.0 \times 10^{-5}$	
R3	$BrO_3^- + Br^- + 2H^+ \rightleftarrows HBrO_2 + HOBr$	$k_{3f} = 2.0$	30
		$k_{3f} = 3.2$	
R4	$2HBrO_2 \rightleftarrows BrO_3^- + HOBr + H^+$	$k_{4f} = 781$	32
		$k_{4r} = 1.0 \times 10^{-8}$	
R4b	$HBrO_2 + H_2BrO_2^+ \rightarrow BrO_3^- + HOBr + 2H^+$	$k_{4'f} = 1013/0.02 = 50650$	32
R5a	$BrO_3^- + HBrO_2 + H^+ \rightleftarrows Br_2O_4 + H_2O$	$k_{5af} = 48$	35
		$k_{5ar} = 3.2 \times 10^3$	
R5b	$Br_2O_4 \rightleftarrows 2BrO_2^{\bullet}$	$k_{5bf} = 7.5 \times 10^4$	35
		$k_{5br} = 1.4 \times 10^9$	
R6	$BrO_2^{\bullet} + Fe(phen)_3^{2+} + H^+ \rightleftarrows HBrO_2 + Fe(phen)_3^{3+}$	$k_{6f} = 1.0 \times 10^9$	30
		$k_{6r} = 33$	
R8a	$Br_2 + MA(enol) \rightarrow BrMA + Br^- + H^+$	$k_{8af} = 2.0 \times 10^6$	33
R8b	$HOBr + MA(enol) \rightarrow BrMA + H_2O$	$k_{8bf} = 6.7 \times 10^5$	33
R9	$Fe(phen)_3^{3+} + BrMA \rightleftarrows P1 + Fe(phen)_3^{2+} + Br^- + 2H^+$	$k_{9f} = 10$	36
		$k_{9r} = 1.0$	
R10	$Fe(phen)_3^{3+} + MA \rightarrow P2 + H^+ + Fe(phen)_3^{2+}$	$k_{10f} = 0.0024$	34
E	$MA \rightleftarrows MA(enol)$	$k_{Ef} = 2.6 \times 10^{-3}$	37
		$k_{Er} = 180$	
A1	$H_2BrO_2^+ \rightleftarrows HBrO_2 + H^+$	$k_{A1f} = 1.0 \times 10^8$	31
		$k_{A1r} = 1.5 \times 10^8$	

on the period time of the iron-catalyzed BZ reaction and showed that the period time decreases exponentially with increasing acidity in the range $0.3-1.4$ mol L^{-1} H_2SO_4.[38] A decrease in the period time with increasing acidity was also reported for the cerium-catalyzed reaction by Misra et al.[39] with initial H_2SO_4 concentrations up to 4.0 mol L^{-1} and by Hsu and Jwo in the acidity range $0.5-1.5$ mol L^{-1} H_2SO_4.[40] The acid dependence usually has been associated with the bromine chemistry of reactions R1−R5. The oxybromine chemistry described by reactions R1−R3 has been known to be accelerated by increased acidity, and it was known long before the initial discovery of the BZ reaction that the rate of R3f is second-order in $[H^+]$.[41] The disproportionation of bromous acid $2HOBrO \rightarrow HOBr + BrO_3^- + H^+$ plays a prominent role as "reaction 4" (or R4 for short) because it is the determining step for the onset of the catalyst oxidation with $r_4 = k_{4f}[HOBrO]^2$, and this reaction was considered to involve two neutral $HBrO_2$ molecules. The reaction rate constant k_{4f} was measured under many conditions by various groups with estimates of k_{4f} ranging over *seven* magnitudes from $4 \times 10^{+8}$ to 39 M^{-1} s^{-1}, and these studies[42−44] have been reviewed (cf. Table 1 in ref 45). Motivated by this disagreement in the value of the rate constant for R4, Glaser and Jost[45] studied the thermochemistry and the kinetics of the HOBrO disproportionation reaction $2HOBrO \rightleftarrows HOBr + HBrO_3$ (reaction R4′) in the gas phase and in aqueous solution

using ab initio theory, and the computed reaction rate constant $k_{4f} = 667.5$ M^{-1} s^{-1} is in excellent agreement with experimental measurements of $k_{4f} = 781 \pm 6$ M^{-1} s^{-1} in neutral and slightly acidic media. However, Försterling and Varga discovered a faster mechanism for $HBrO_2$ disproportionation that involves the reaction of one neutral $HBrO_2$ with a protonated species $H_2BrO_2^+$, reaction R4b.[31] A value of 1.7×10^5 M^{-1} s^{-1} was assigned to the rate constant of R4b, and the adjustable parameter of 0.02 M^{-1} was used as the equilibrium constant for the protonation reaction $HBrO_2 + H^+ \rightleftarrows H_2BrO_2^+$. Agreda and Field[32] showed the overall rate of $HBrO_2$ disproportionation to be consistent with both reactions R4 and R4b occurring in parallel, and they refined the rate constant for R4b to the value 1013 ± 16 M^{-1} s^{-1}.

In this article, we report the results of an analysis of the acidity dependence of the iron-catalyzed bromate-malonic acid Belousov−Zhabotinsky reaction by video-based tracing of the time-dependent concentration of the Fe(III) catalyst and of simulations of the same reaction systems using kinetic rate equations. The initial conditions of Shakashiri[46] were employed, and the sulfuric acid concentration was varied (Table 2). The effects of the acidity on the temporal evolution of period times, oxidation times, and reduction times as well as of the intensity variations were quantified. Each reaction was studied with sodium and potassium salts. No significant differences were observed using Na^+ and K^+ salts, and we

Table 2. Initial Reaction Conditions and Reaction Naming Convention[a]

BZ reaction with K$^+$ salts	BZ reaction with Na$^+$ salts	H$_2$SO$_4$ [M]	pH
KM036	NaM036	0.360	0.443
KM041	NaM041	0.408	0.389
KM043	NaM043	0.432	0.364
KM048	NaM048	0.481	0.318
KM053	NaM053	0.529	0.277
KM055	NaM055	0.553	0.258
KM060	NaM060	0.601	0.221
KM062	NaM062	0.625	0.204
KM065	NaM065	0.649	0.188
KM072	NaM072	0.721	0.142
KM077	NaM077	0.769	0.114
KM084	NaM084	0.841	0.075
KM089	NaM089	0.889	0.051
KM096	NaM096	0.961	0.017
KM108	NaM108	1.081	−0.034
KM120	NaM120	1.201	−0.080

[a]All reactions employed $[MA]_0 = 100.5$ mM and $[Fe]_0 = 0.297$ mM. Reactions KM%%% employed potassium salts: $[KBrO_3]_0 = 74.36$ mM, $[KBr]_0 = 19.22$ mM. Reactions NaM%%% employed potassium salts: $[NaBrO_3]_0 = 73.63$ mM, $[NaBr]_0 = 19.06$ mM. Approximate pH computed by pH $= -\log_{10}[H_2SO_4]_0$.

report the data for the potassium series. Our measurements show a very strong inverse dependence of period time on acidity, and the period times decrease exponentially with acidity. While we were motivated by our interest in the HBrO$_2$ disproportionation chemistry, the numerical simulations showed relatively quickly that the acid dependence of R4 has only a minor effect on the overall dynamics of the BZ reaction. Instead, and unexpectedly, we found that agreement between the experiments and their simulations can only be achieved with the inclusion of proton-catalysis of the outer shell electron transfer reaction between the oxidized species $[Fe(phen)_3]^{3+}$ and bromomalonic acid in reaction 9 (reaction R9). The simulation of reaction R9 with a second-order dependence on $[H^+]$ results in compelling agreement with experiment over the entire range of acidities measured. An explanation is offered for this catalysis based on the acidity dependence of the ion aggregation of the oxidant and its effect on that rate of electron transfer.

■ EXPERIMENTAL AND MATHEMATICAL METHODS

Performance and Recording of Oscillating Reactions. We followed the protocol by Shakashiri[46] for the iron- and cerium-catalyzed bromate-malonic acid reaction except we omitted the cerium. We prepared three solutions. The first beaker contained 250 mL of DI (deionized) water and 9.5 g (56.886 mmol, MM(KBrO$_3$) = 167.00 g/mol) of potassium bromate (KBrO$_3$, Acros Organics, 99.5%). The second beaker contained 250 mL of DI water, 1.75 g (14.71 mmol, MM(KBr) = 119.00 g/mol) of potassium bromide (KBr, Acros Organics, 99+%), and 8.0 g (0.077 mol, MM(MA) = 104.06 g/mol) of malonic acid (MA, H$_2$C(COOH)$_2$, Acros Organics, 99%). The third beaker contained a varied volume of 18.38 M sulfuric acid (H$_2$SO$_4$, Fischer Scientific, 96.5%) and enough DI water to make the total volume of the third beaker 250 mL. We varied the concentration of H$_2$SO$_4$ by adding a different volume of acid to a graduated cylinder and adding enough water to afford

250 mL of the acid solution. All three of these beakers contained 250 mL of solution. We also made a fresh ferroin solution by mixing 100 mL of DI water, 0.23 g (1.51 mmol) of iron(II) sulfate heptahydrate (FeSO$_4$·(H$_2$O)$_7$, Sigma-Aldrich, 99.999%), and 0.46 g (1.96 mmol) of 1,10-phenanthroline (Sigma-Aldrich, 99+%).

In a 1 L beaker on a stir plate, we mixed the first two solutions, added the third solution, and then added 15 mL of the ferroin solution. Final concentrations in the 1 L beaker were 74.36 mM KBrO$_3$, 0.10 M MA, 19.22 mM KBr, 0.90 M H$_2$SO$_4$, and 0.297 mM in Fe(II). A summary of the initial reaction conditions is given in Table 2. Reactions are labeled KM%%%, where the "K" indicates that potassium salts were used and "M%%%" indicates the molarity of H$_2$SO$_4$ multiplied by 100. For example, the reaction KM120 employs an initial H$_2$SO$_4$ concentration of 1.20 M. In analogy, the labels "NaM%%%" refer to reactions with sodium salts.

The reaction was recorded with a Panasonic HC-V110 video camera which was mounted on a tripod set about five feet away from the reaction beaker. A white poster board was placed behind the reaction beaker, and lighting conditions were kept constant. The zoom on the camera was set to 5×. The reaction was recorded for approximately 40 min. HD Writer 2.0 was used to edit the video in the form iFrame and produce an mp4 file.

Video Analysis and Generation of Raw Data. The mp4 video is first converted to a series of JPEG images using the Aoao Video to Picture Converter[47,48] using a standard of 5 frames per second. Next, the images are imported into Mathematica,[49,50] software for image analysis. The images are cropped to isolate the desired region (not obstructed, middle of the beaker, avoiding vortex regions) and converted to matrices of Red−Green−Blue-values using the ImageData command in Mathematica.

The next step is the choice of a metric to integrate all the data points in the cropped image and compare them to a given target value. For a given image with frame number FN and corresponding to reaction time $t = FN/FPS$, we chose the average relative distance from our characteristic color target values using the formula:

$$DCC(t, R_c, G_c, B_c) = 1 - l^2 norm$$
$$= 1 - \sum_1^m \sum_1^n (id(i, j, 1) - R_c)^2$$
$$+ (id(i, j, 2) - G_c)^2$$
$$+ (id(i, j, 3) - B_c)^2$$

Here, id is a $m \times n \times 3$ matrix which contains the Red-, Green-, and Blue-values at each of the $m \times n$ points of the cropped image.

The constant target values R_C, G_C, and B_C are the Red-, Green-, and Blue-values predetermined to make the ideal target color. This formula evaluates the deviation from the ideal color, where the value of one indicates no deviation. Consequently, once the color of the pure indicator at an oxidation state is known, the target R_C, G_C, and B_C values can be set, and the relative concentration of that oxidation state is recorded over time using the described method. In the present study we determined the $DCC(t)$ time traces for the blue color resulting from a high concentration of oxidized iron catalyst (ferriin, Fe(phen)$_3^{3+}$) utilizing the RGB standard values 0.072606, 0.187665, and 0.390992 for R, G, and B,

respectively. The sum of the RGB values has been used in an analogous way to Beer's Law to calculate species concentrations.[51−56] A Fourier transform has been applied to the RGB data,[57] and a digital image-based method has been employed to determine the end point of titrations.[58,59] A similar approach to ours, using the square of a difference from a standard or reference color, has also been used as a way of extracting concentrations from RGB data.[60] Video analysis was used to track chemical waves in a 2D BZ system by comparing ratios of intensities to a standard in Beer's Law with different back lighting conditions.[61]

Our approach follows the concept described by Beer's Law. The basic assumption is made that one might be able to recover information on the variation of the concentrations of individual species based on the variation of the color of the solution. For example, one would expect that a blue color corresponds to a high concentration of Fe(III) whereas a deep red solution would correspond to a high concentration of Fe(II).

Oscillation Pattern Analysis. We are interested in quantifying the timing of the oscillations and the intensity variations over the course of each reaction. Variations in the timing and intensities of the oscillations and $DCC(t)$ time traces will allow us to construct parameters to describe the oscillations and elucidate mechanistic details and effects of acidity. The determination of these oscillation parameters requires the knowledge of the minima and maxima of the $DCC(t)$ time traces (Scheme 1).

Scheme 1. Definition of the Oscillation Parameters $DCC_{min}(t)$, $DCC_{max}(t)$, $PT_{max}(t)$, $PT_{min}(t)$, $OT(t)$, and $RT(t)$
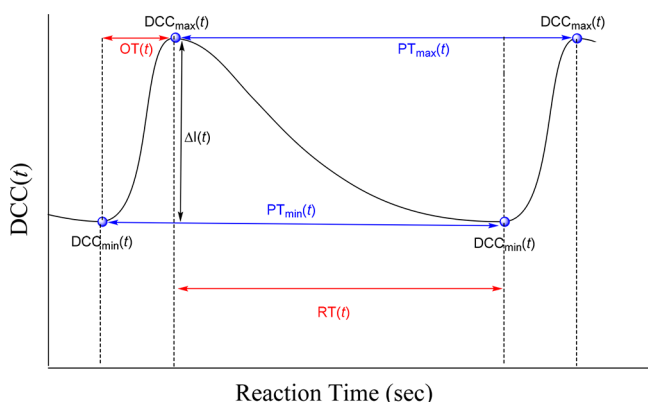
In this article we focus on the timing of the oscillations, and for completeness we provide a discussion of acidity effects on intensity variations in Supporting Information. We are studying the period time as measured using both the maxima (PT_{max}) and the minima (PT_{min}), the oxidation times (OT) as calculated by the time of the maximum minus the time of the preceding minimum, and the reduction times (RT) as calculated by the time of the minimum minus the time of the preceding maximum. The selection and calculation of these parameters are shown in Scheme 1.

The raw discrete $DCC(t)$ data are too noisy to work with and needs to be smoothed. After smoothing of the $DCC(t)$ data using a moving average filter, local minima and maxima of $DCC(t)$ can be located with an extrema-point finder function ($EPmax(t)$ and $EPmin(t)$ for maxima and minima, respec-

tively), and a list of minima and maxima points (time, $DCC(t)$ value) is generated. This method is inadequate for our analysis, however, because the minima and maxima points extracted by this method do not represent the true minima and maxima of the oscillation cycle. In some reactions, especially those with a longer period time, the point with the lowest $DCC(t)$ value occurs long before the beginning of the oxidation phase and can show considerable variation between periods. We define the minimum point as the point at which the oxidation phase begins, and in order to accomplish this, we had to develop an additional analysis method. This method consists of first generating an interpolation function of the smoothed $DCC(t)$ data and then looking for the minima by starting at the maxima and moving in the negative time direction until the derivative became a certain predetermined value ($dDCC(t)/dt = 60$).

A slightly different problem occurred in determining the maxima points. The $DCC(t)$ values come as discrete points at time intervals of 0.2 s, and for reactions with sharper peaks, it is possible that the actual maximum of the oscillation cycle falls between the measured discrete points. This would not normally be a very large problem for extracting the timing information of the oscillations (i.e., 0.2 s is a relatively small error for the time scale of the oscillations), but if accurate $DCC(t)$ values of the maxima are desired simply taking the $EPmax(t)$ values could result in a relatively large error between the $EPmax(t)$ value and the actual maximum value of the oscillation cycle. To reduce this error the maxima points were chosen as the maxima of the interpolation function of the smoothed $DCC(t)$ data.

Mathematical Simulation of the Oscillating Reaction. We have previously described a dynamical method for the calculation of all species concentrations in multiequilibria systems,[62−64] and this method can be used to examine the transient kinetics of the evolution of the BZ reaction chemistry. The dynamical method has its basis in general mass action kinetics theory[65] and results in the formulation of differential equations representing the derivatives of species concentrations with respect to time. We solved the resulting system of differential equations using the NDSolve[66] command in *Mathematica*[49,67] and obtained concentration data for all chemical species in the system over the entire selected time range.

■ RESULTS AND DISCUSSION

Qualitative Description of the Temporal Evolution of the Oscillation Pattern. Three representative $DCC(t)$ time traces are shown in Figure 1 for the reactions with initial sulfuric acid concentrations $[H_2SO_4]_0$ of 1.20, 0.89, and 0.48 mol L^{-1}, respectively. Figure 2 shows the same $DCC(t)$ time traces with increased temporal resolution, that is, over a smaller time range of 300 s between 1300 and 1600 s of reaction time.

Figures 1 and 2 clearly show that the oscillation frequencies increase with the acidities of the reactions. In addition, Figure 2 shows that in reactions at lower acidities the $DCC(t)$ values rapidly decrease and stay near the minimum until the next oxidation phase. Another effect that can be seen in Figure 1 is that the $DCC(t)$ values remain higher at higher acidities whereas the difference $\Delta I(t)$ between the values at the maximum and the minimum is greater at lower acidities.

The change in PT_i as well as OT and RT over time is examined further in Table 3 which shows the parameters PT_{min}, PT_{max}, OT, and RT at $t = 500$ and $t = 2000$ s. For most

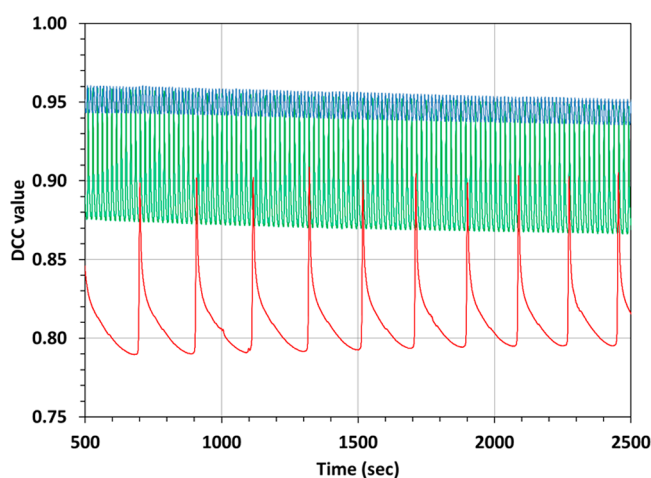**Figure 1.** DCC values over time (500−2500 s) for reactions KM120 (blue), KM089 (green),and KM048 (red).
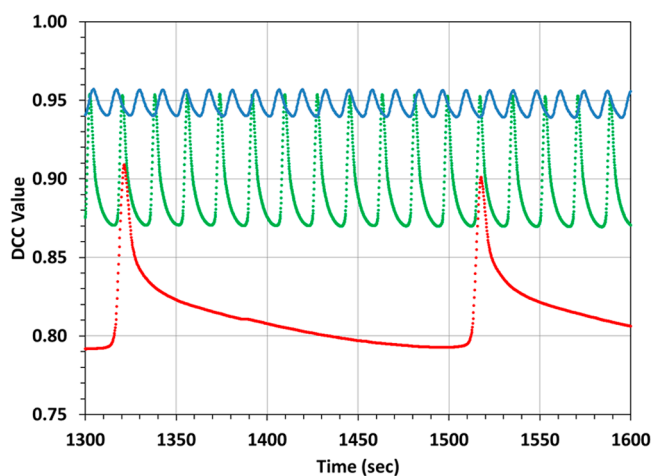

Figure 2. DCC values over time (1300−1600 s) for reactions KM120 (blue), KM089 (green), and KM048 (red).

reactions the induction period is over by 500 s of reaction time, and all reactions were performed for at least 2000 s. The $PT_i(2000)$ is greatest at the lowest acidity and smallest at the highest acidity. It can also be seen in Table 3 that the PT_i increases over time for reactions performed at higher acidities and decreases over time for reactions performed at lower acidities. For the reactions performed at the lowest acidities ($[H_2SO_4]_0 \leq 0.48$ mol L^{-1}), the first period was not observed until after 500 s of reaction time so the $t = 500$ cells in Table 3 for those reactions are left blank. Similar trends were also observed in the OT and RT. A shorter OT is seen at higher acidities, consistent with the trend in PT_i. The difference in OT at low acidities and high acidities is, however, not very large, and the OT does not become smaller as consistently as the PT_i. Moreover, the OT does not change significantly or consistently over time. Additionally, the OT represents a greater proportion of the overall PT_i at higher acidities compared to lower acidities. The RT follows trends similar to that of the PT_i in that it becomes shorter at higher acidities and the $RT(2000)$ is greater than the $RT(500)$ at higher acidities, but this relation is reversed at lower acidities. The RT represents a greater proportion of the overall PT_i than the OT at lower acidities with the RT and OT becoming closer in value at higher acidities.

Quantification of the Temporal Evolution of Oscillation Timing. The trends suggested in Figures 1 and 2 regarding period time, the shape of the curves, and the average $DCC(t)$ value as well as Table 3 motivated us to systematically study different parameters to describe the oscillations as they are affected by changes in acidity or if perhaps such parameters will change over the course of one reaction. As an example, the $PT_{max}(t)$, $PT_{min}(t)$, $OT(t)$, and $RT(t)$ values with their respective linear regression lines for the reaction KM089 are plotted in Figure 3 as a function of time. Plots analogous to Figure 3 for all other reactions are given in the Supporting Information (Figure S1).

In Figure 3 it can be seen that the values $PT_{max}(t)$ and $PT_{min}(t)$ are about the same at any given time t and that both values increase slightly but noticeably over the course of the

Table 3. Reaction Parameters $PT_{min}(t)$, $PT_{max}(t)$, $OT(t)$, and $RT(t)$ at $t = 500$ s and $t = 2000$ s

reaction	$PT_{min}(t)$		$PT_{max}(t)$		$OT(t)$		$RT(t)$	
	$t = 500$	$t = 2000$	$t = 500$	$t = 2000$	$t = 500$	$t = 2000$	$t = 500$	$t = 2000$
KM036	a	494.6[b]		496.4		14.2		482.2
KM041		482.0		483.1		15.2		467.8
KM043		336.2		337.7		15.9		321.8
KM048		184.2	212.1	187.3	12.9	14.4	199.2	172.9
KM053	86.3	75.6	84.5	75.5	7.6	8.3	76.9	67.2
KM055	89.5	79.4	88.9	80.6	8.7	9.0	80.2	71.6
KM060	83.4	75.8	81.5	7.6	7.1	8.6	74.4	68.0
KM062	57.7	60.0	58.7	59.3	8.2	7.0	54.5	52.3
KM065	41.7	41.7	42.3	42.9	7.2	7.9	35.1	35.0
KM072	32.2	32.8	31.8	32.9	6.5	7.4	25.3	25.5
KM077	21.7	22.6	21.8	22.6	4.7	4.6	17.2	18.0
KM084	21.1	23.4	21.1	22.8	5.4	5.3	15.7	17.6
KM089	17.1	18.7	17.3	18.1	4.4	4.1	12.8	14.0
KM096	9.2	9.9	9.2	10.0	4.4	4.6	4.8	5.4
KM108	11.8	13.3	11.7	13.4	5.1	5.5	6.7	7.9
KM120	8.1	9.1	8.2	9.3	4.1	4.5	4.1	4.6

[a]Reactions with lower initial sulfuric acid concentration sometimes did not exhibit a first oscillation until after 500 s of reaction time. [b]Parameter values were chosen on the basis of the proximity of their time (absolute value) from $t = 500$ s or $t = 2000$ s.
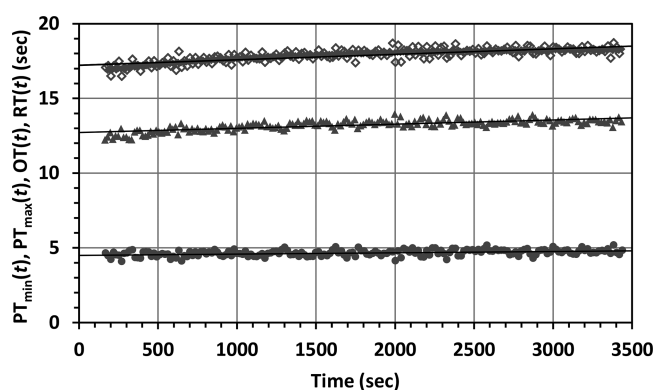
Figure 3. Values of $PT_{min}(t)$, $PT_{max}(t)$, $OT(t)$, and $RT(t)$ as a function of reaction time t for reaction KM089 (green in Figures 1 and 2). Unfilled diamonds indicate $PT_{min}(t)$, and filled diamonds indicate $PT_{max}(t)$. Circles indicate $OT(t)$, and triangles indicate $RT(t)$. The regression lines also are shown for $PT_{min}(t) = m_1 t + PT_1(0)$, $PT_{max}(t) = m_2 t + PT_2(0)$, $OT(t) = m_3 t + OT(0)$, and $RT(t) = m_4 t + RT(0)$.

reaction. The $OT(t)$ values, the lowest curve in Figure 3, remain essentially the same over time. Hence, the $RT(t)$ values follow the trend for $PT_{max}(t)$ and $PT_{min}(t)$ and also increase slightly but noticeably over time. The temporal evolution of the parameters $PT_{max}(t)$, $PT_{min}(t)$, $OT(t)$, and $RT(t)$ can be modeled by linear regression, and the slopes and intercepts of these linear regressions are given in Table 4 for all reactions. For example, we list the intercept $PT_1(0) = PT_{max}(0)$ and the slope m_1 for the regression function $PT_{max}(t) = m_1 t + PT_1(0)$. Standard correlation coefficients, R^2, and standard errors of the estimate, σ_{est}, are included in Table 4.

It is an oddity of the definition of R^2 that it can become very small when slopes are near zero even though the data do not exhibit much scatter (cf. Figure S1 KM065 and R^2(KM065) = 0.13). Hence, we also determined the standard error of the estimate, σ_{est}, which was calculated by the following formula:

$$\sigma_{est} = \sqrt{\frac{\sum_n (p' - p)^2}{n}}$$

where p' is the estimated parameter value based on the linear regression line, p is the measured parameter value, and n is the

Table 4. Linear Regression for Reaction Parameters $PT_{min}(t)$, $PT_{max}(t)$, $OT(t)$, and $RT(t)$ of KM Reactions

reaction	$PT_{min}(t)$				$PT_{max}(t)$				ΔPT^a
	$PT_1(0)$	$m_1 \times 10^3$	R^2	σ_{est}	$PT_2(0)$	$m_2 \times 10^3$	R^2	σ_{est}	
KM036	639.92	−67.86	0.94	9.21	577.13	−40.94	0.75	16.39	10.88
KM041	543.55	−40.82	0.87	7.87	528.94	−34.17	0.86	9.15	2.76
KM043	377.18	−20.61	0.96	1.90	369.62	−16.60	0.92	2.80	2.04
KM048	224.11	−17.40	0.95	2.85	222.76	−16.71	0.98	2.03	0.60
KM053	86.08	−5.01	0.89	1.24	86.59	−5.29	0.97	0.61	−0.59
KM055	91.31	−5.47	0.91	1.19	91.27	−5.45	0.99	0.47	0.04
KM060	82.39	−2.72	0.80	0.85	82.62	−2.90	0.98	0.26	−0.29
KM062	58.54	0.38	0.15	0.75	58.49	0.41	0.92	0.15	0.09
KM065	42.16	0.37	0.13	0.65	42.09	0.43	0.97	0.07	0.17
KM072	31.52	0.68	0.47	0.55	31.49	0.70	0.98	0.10	0.07
KM077	21.63	0.47	0.38	0.47	21.59	0.50	0.98	0.07	0.21
KM084	20.58	1.16	0.57	0.63	20.59	1.15	0.98	0.12	−0.06
KM089	17.22	0.36	0.60	0.28	17.21	0.37	0.93	0.13	0.07
KM096	8.98	0.47	0.99	0.04	8.98	0.47	1.00	0.03	0.02
KM108	11.30	1.04	0.98	0.11	11.30	1.04	1.00	0.05	0.01
KM120	7.82	0.70	0.99	0.06	7.82	0.70	1.00	0.05	0.02

reaction	$OT(t)$				$RT(t)$			
	$OT(0)$	$m_3 \times 10^3$	R^2	σ_{est}	$RT(0)$	$m_4 \times 10^3$	R^2	σ_{est}
KM036	13.58	1.03	0.13	1.83	562.85	−41.96	0.72	18.13
KM041	17.81	−0.72	0.07	1.75	510.51	−33.41	0.84	9.53
KM043	15.25	−0.19	0.01	1.02	354.11	−16.40	0.89	3.31
KM048	11.39	0.40	0.07	1.09	211.17	−17.11	0.96	2.52
KM053	8.37	0.02	0.00	0.73	78.02	−5.18	0.94	0.93
KM055	9.01	−0.27	0.07	0.71	82.29	−5.22	0.95	0.84
KM060	8.52	−0.14	0.03	0.55	73.91	−2.61	0.86	0.69
KM062	7.36	0.15	0.06	0.50	51.15	0.25	0.14	0.53
KM065	6.74	0.08	0.02	0.41	35.38	0.32	0.22	0.41
KM072	6.72	0.15	0.10	0.35	24.80	0.53	0.58	0.35
KM077	4.79	−0.08	0.03	0.36	16.80	0.57	0.57	0.39
KM084	5.12	0.23	0.10	0.44	15.47	0.93	0.59	0.49
KM089	4.49	0.09	0.17	0.19	12.72	0.28	0.57	0.23
KM096	4.35	0.12	0.94	0.03	4.63	0.35	0.99	0.03
KM108	5.02	0.25	0.87	0.07	6.29	0.79	0.98	0.08
KM120	3.99	0.26	0.95	0.05	3.84	0.44	0.98	0.05

$^a\Delta PT = \{PT_1(0) - PT_2(0)/PT_2(0)\} \times 100\%$.

number of values for the parameter. Comparison of the σ_{est} value to the intercept $PT_1(0)$ for any given reaction shows less than 3% deviation, and the quality of the fit is equally high for the regressions of the $PT_{min}(t)$ and $RT(t)$ data. Another approach to estimate numerical error consists of the pairwise comparison of the intercepts $PT_1(0)$ and $PT_2(0)$. In an ideal world, one would expect that the period times determined with the $PT_{min}(t)$ and $PT_{max}(t)$ data, respectively, are exactly the same, i.e., $PT_1(0) = PT_2(0)$. The data in Table 4 show that $PT_1(0) \neq PT_2(0)$, and the difference can become quite large in absolute value. However, the relative deviation $\Delta PT = \{PT_1(0) - PT_2(0)/PT_2(0)\} \times 100\%$ again remains below 3% with the single exception of reaction KM036 (only 4 oscillations measured).

Acidity Dependence of Oscillation Timing. The dependence of the $PT_i(0)$ values and of the associate slopes m_i on the initial sulfuric acid concentration $[H_2SO_4]_0$ is illustrated in Figure 4. Figure 4 clearly shows that $PT_i(0)$
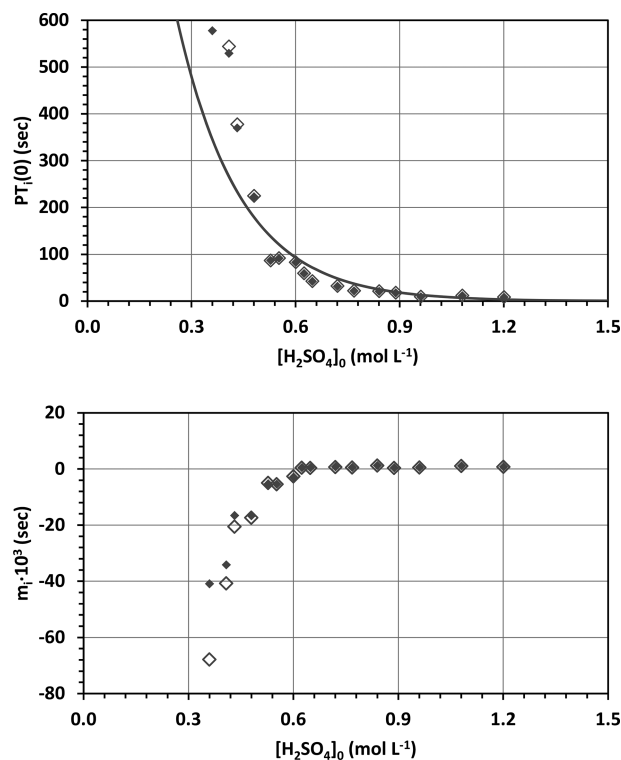

Figure 4. Period length variations of the KM series of reactions depending on sulfuric acid concentration. Values of $PT_i(0)$ (top) and of $m_i \times 10^3$ (bottom) are shown as a function of initial sulfuric acid concentration $[H_2SO_4]_0$. Unfilled diamonds indicate $PT_1(t)$ and m_1 values, and filled diamonds indicate $PT_2(t)$ and m_2 values. An exponential regression curve is also plotted for the $PT_1(0)$ data.

decreases with increasing acidity. There is a steep decrease in $PT_i(0)$ in the region $0.3 < [H_2SO_4]_0 < 0.6$, and $PT_i(0)$ asymptotically approaches zero in the region $[H_2SO_4]_0 > 0.9$. In the bottom plot of Figure 4, it can be seen that the slopes m_1 and m_2 increase with $[H_2SO_4]_0$. The magnitude of the slopes all are small (<0.1), but they show significant features. Interestingly, the sign of the slopes changes from negative to positive in the region $[H_2SO_4]_0 \approx 0.6$. Note that the slopes m_1 and m_2 increase relatively rapidly in the region $[H_2SO_4]_0 < 0.6$ (m_1 from −0.067 to −0.0027; m_2 from −0.041 to −0.0029) while the slope remains essentially constant, very small, and

slightly positive ($m_1 < +0.0015$) in the high-acidity region $[H_2SO_4]_0 > 0.6$. Thus, the period times PT_i decrease over the course of the reaction at lower acidities, and the decrease is more pronounced at lower acidities. On the other hand, the PT_i increases over the course of a reaction when $[H_2SO_4]_0 > 0.6$, and this increase in PT_i is relatively constant and low over the remaining range of initial sulfuric acid concentrations. The observed dependence of the period times reflects the acidity dependence of the reduction phase of the oscillating reaction.

The $RT(0)$ values (top) and the slopes m_3 (bottom) are plotted in Figure 5 as a function of the initial sulfuric acid
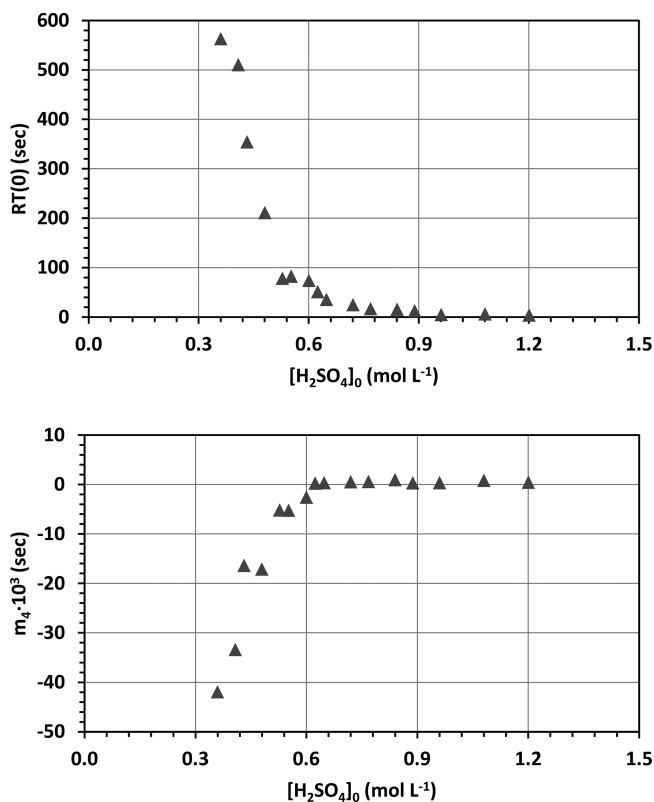
Figure 5. Variation of reduction times $RT(0)$ (top) and of $m_4 \times 10^3$ (bottom) of the KM series of reactions depending on the initial sulfuric acid concentration $[H_2SO_4]_0$.

concentration $[H_2SO_4]_0$. The plot of $RT(0)$ as a function of $[H_2SO_4]_0$ closely resembles the respective plot of PT_i in Figure 4. The $RT(0)$ values are high at low acidity and approach an asymptote with increasing acidity. As with the $PT_i(0)$ values in Figure 4, the greatest decrease in $RT(0)$ occurs in the region $0.3 < [H_2SO_4]_0 < 0.6$, and the $RT(0)$ values are fairly constant and low in the region $0.9 < [H_2SO_4]_0 < 1.2$. The bottom part of Figure 5 also shows the same effect of acidity as with the PT_i values. Just like the slopes m_1 and m_2 of the plots $PT_i(t) = m_i t + PT_i(0)$, the slope m_4 describing $RT(t) = m_4 t + RT(0)$ starts negative, increases rapidly to a positive value at $[H_2SO_4]_0 = 0.6$, and remains constant and slightly positive as $[H_2SO_4]_0$ increases.

Figure 6 shows the $OT(0)$ values as a function of the initial sulfuric acid concentration $[H_2SO_4]_0$. The $OT(0)$ values decrease with increasing $[H_2SO_4]_0$ and asymptotically approach the value of about 4 s. The changes of m_3 with increasing $[H_2SO_4]_0$ are insignificant (Table 3) and are not included in Figure 6. The data suggest that the oxidation time
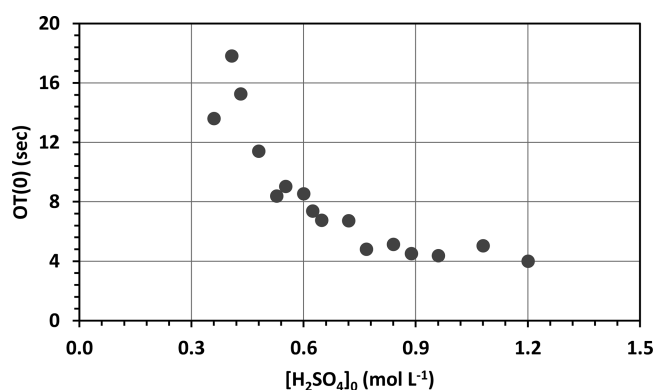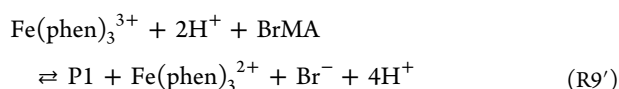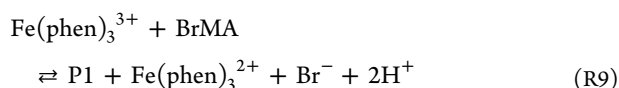
Figure 6. Variation of oxidation times OT(0) of the KM series of reactions depending on the initial sulfuric acid concentration $[H_2SO_4]_0$.

OT does not depend to a significant extent on acidity and does not contribute to the significant changes of the period times PT_i as the acidity is varied. At the lower acidities the OT is a very small proportion of the PT_i whereas at higher acidities the OT can make up as much as one-half of the total PT_i.

Because the acidity effects on the period times PT_i are so similar to those on the reduction RT, it can be concluded that the acidity dependence of the period times PT_i are primarily due to the acidity dependence of the reduction phase of the BZ reaction. Hence, the question becomes why the reduction time RT becomes shorter and shorter with increasing acidity and accounts for less and less of the total period time PT_i.

Numerical Simulation of the Belousov–Zhabotinsky Reaction. In order to understand the effect of acidity on the kinetics of the BZ reaction, a simulation of the entire reaction was necessary and the standard set of reactions did not match experimental results across the acidity range studies. The simulation based on the reactions of the core mechanism with the reactions listed in Table 1 and in combination with the initial conditions of Table 2 (the BZR1 system) did *not* produce oscillations at acidities of $[H_2SO_4]_0 < 0.8$ mol L^{-1}. In the acidity range where this BZR1 system did feature oscillations, the acidity dependence of the simulated period times did *not* resemble the experimental data even in a qualitative fashion (vide infra). We explored many chemically plausible variations of the reactions of the core mechanism, and the simulations met with success only when we changed the forward reaction R9 in the BZR1 system to include a second-order dependence on $[H^+]$ in the modified reaction R9′ in the BZR2 system.

$$Fe(phen)_3^{3+} + BrMA$$
$$\rightleftharpoons P1 + Fe(phen)_3^{2+} + Br^- + 2H^+ \quad (R9)$$

$$Fe(phen)_3^{3+} + 2H^+ + BrMA$$
$$\rightleftharpoons P1 + Fe(phen)_3^{2+} + Br^- + 4H^+ \quad (R9′)$$

The consideration of this $[H^+]$ dependence on reaction R9 was not at all obvious. The omission of this $[H^+]$ dependency usually is inconsequential because acid concentrations in typical BZ reactions are $[H^+] \approx 1$ M. The success of the addition of this $[H^+]$ dependence is undeniable, however, as not only does the BZR2 system produce oscillations over the entire experimental acidity range but also the period lengths of

the simulations match the measured period lengths in a compelling fashion.

As an example, Figure 7 illustrates the oscillations of the concentration of $HBrO_2$ as a function of time for the
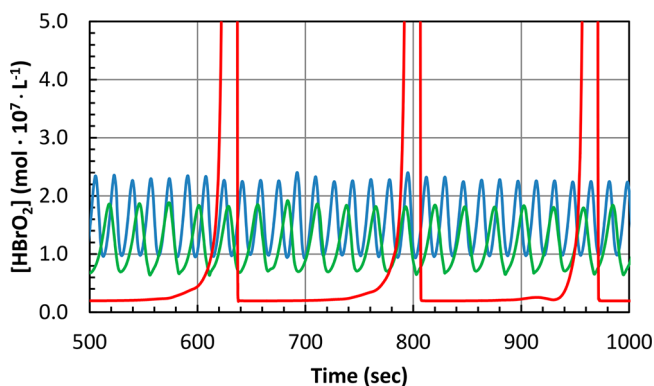
Figure 7. Simulated concentrations (mol L^{-1}) of $HBrO_2$ as a function of time (t, in s) for the simulation system BZR2 with constant initial conditions $[BrO_3^-]_0 = 0.07436$ mol L^{-1}, $[Br^-]_0 = 0.01922$ mol L^{-1}, $[MA]_0 = 0.1$ mol L^{-1}. The initial sulfuric acid concentration was varied, and the $[HBrO_2](t)$ traces are shown for the three acidities $[H_2SO_4]_0 = 1.20$ mol L^{-1} (blue), $[H_2SO_4]_0 = 0.89$ mol L^{-1} (green), and $[H_2SO_4]_0 = 0.48$ mol L^{-1} (red) corresponding to the experimental systems KM120, KM089, and KM048, respectively. The $[HBrO_2](t)$ trace for $[H_2SO_4]_0 = 0.48$ mol L^{-1} (red) has concentration maxima on the order of 1.35×10^{-5} mol L^{-1}.

simulation of the BZR2 system at 0.48, 0.89, and 1.20 M H_2SO_4. The determination of the oscillation parameters characterizing the oscillations resulting in the BZR2 simulation was accomplished with the same method described for the analysis of the experimental data. The temporal evolution of the parameters $PT_{max}(t)$, $PT_{min}(t)$, $OT(t)$, and $RT(t)$ were modeled by linear regression for all acidities, and the slopes and intercepts obtained by these linear regressions are given in Table 5. For example, we list the intercept $PT_1(0) = PT_{max}(0)$ and the slope m_1 for the regression function $PT_{max}(t) = m_1t + PT_1(0)$. Standard correlation coefficients, R^2, and the standard errors of the estimate, σ_{est}, are included in Table 5.

The most important parameter is the period time, and the simulated PT_i data are compared to the experimental data in Figure 8. The black line shows the exponential regression curve fit to the measured period lengths. The BZR1 simulation (blue in Figure 8) oscillates only at $[H^+] > 0.9$ mol L^{-1} and would suggest that the period lengths increase with acidity. In sharp contrast, the BZR2 simulation (green in Figure 8) not only oscillates over the entire acidity range but also matches the experimental period times in a stunning fashion. Comparisons of the simulated reduction times RT and oxidation times OT with the measured data are illustrated in Figure S3, and they also match very well.

Ion-Pairing Effects on Electron Transfer Reaction. We were able to replicate the acidity effect on the period times in a compelling fashion by replacement of forward reaction R9 by way of inclusion of a second-order dependence on $[H^+]$ in the modified forward reaction R9′. How exactly this occurs mechanistically is still unclear, but literature on electron transfer reactions between transition metal complexes suggests a plausible explanation. There is evidence that oxidations by $[Fe(phen)_3]^{3+}$ species involve outer sphere electron transfer.[68] The suggested proton-dependence of the oxidation of BrMA

Table 5. Linear Regression for Reaction Parameters $PT_{min}(t)$, $PT_{max}(t)$, $OT(t)$, and $RT(t)$ of BZR2 Simulation

$[H_2SO_4]_0$ [b]	$PT_{min}(t)$				$PT_{max}(t)$				ΔPT [a]
	$PT_1(0)$	$m_1 \times 10^3$	R^2	σ_{est}	$PT_2(0)$	$m_2 \times 10^3$	R^2	σ_{est}	
0.30	329.59	63.93	1.00	0.00	408.13	22.09	0.77	0.00	19.25
0.40	252.88	−2.65	0.04	0.00	255.21	−4.94	0.14	6.35	0.91
0.50	162.88	−2.91	0.10	4.13	160.14	−2.66	0.20	3.93	0.07
0.60	109.50	−0.08	0.01	2.70	110.21	−0.38	0.12	2.61	0.64
0.65	93.95	0.48	0.06	2.36	94.35	0.34	0.04	2.30	0.48
0.75	74.08	−0.77	0.28	2.46	73.00	−0.13	0.00	2.37	0.11
0.85	33.09	−2.54	0.22	0.73	34.41	−3.46	0.20	0.72	3.85
0.90	28.33	−1.17	0.24	0.65	28.98	−1.62	0.20	0.65	2.19
1.00	23.01	−0.46	0.30	0.54	23.20	−0.58	0.22	0.54	0.71
1.10	19.47	−0.17	0.10	0.46	19.56	−0.21	0.12	0.45	0.34
1.20	17.16	−0.12	0.08	0.40	17.19	−0.14	0.13	0.40	0.18
1.30	15.34	−0.06	0.01	0.36	15.35	−0.07	0.05	0.36	0.04
1.40	13.89	0.02	0.00	0.32	13.88	0.02	0.01	0.33	0.06
1.50	12.65	0.13	0.05	0.30	12.64	0.14	0.06	0.30	0.10

$[H_2SO_4]_0$	$OT(t)$				$RT(t)$			
	$OT(0)$	$m_3 \times 10^3$	R^2	σ_{est}	$RT(0)$	$m_4 \times 10^3$	R^2	σ_{est}
0.30	50.24	36.23	0.80	0.00	339.29	−3.93	1.00	0.00
0.40	72.97	1.35	0.01	3.44	186.04	−9.19	0.78	0.00
0.50	50.06	1.57	0.07	2.25	110.72	−4.86	0.75	3.39
0.60	37.02	2.93	0.90	1.57	72.80	−3.14	0.98	2.16
0.65	33.18	3.39	0.80	1.43	61.00	−3.01	0.99	1.85
0.75	28.28	3.91	0.83	1.54	44.59	−4.03	0.99	1.87
0.85	17.24	−1.14	0.19	0.53	15.81	−1.38	0.23	0.50
0.90	15.19	−0.65	0.28	0.47	13.14	−0.51	0.16	0.44
1.00	12.34	−0.21	0.18	0.39	10.69	−0.25	0.22	0.36
1.10	10.56	−0.13	0.14	0.34	8.92	−0.02	0.01	0.32
1.20	9.28	−0.14	0.21	0.29	7.88	0.02	0.01	0.27
1.30	8.24	−0.15	0.19	0.26	7.11	0.08	0.04	0.25
1.40	7.37	−0.09	0.13	0.23	6.52	0.11	0.07	0.22
1.50	6.62	−0.05	0.04	0.22	6.03	0.18	0.16	0.21

[a] $\Delta PT = \{PT_1(0) - PT_2(0)/PT_2(0)\} \times 100\%$. [b] $[H^+]_0 = [H_2SO_4]_0$.
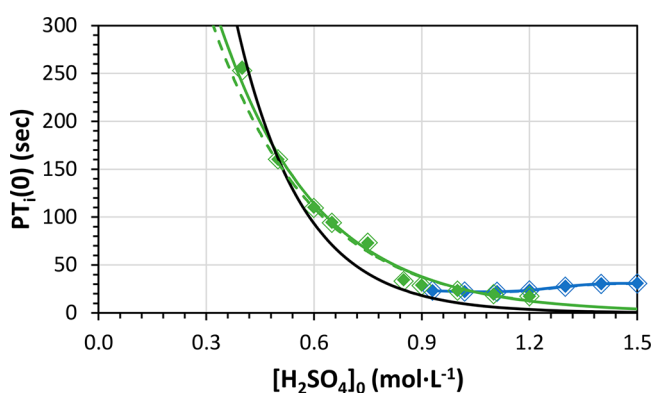
Figure 8. Period length variations of the simulation BZR1 (blue), BZR2 (green), and the exponential regression curve of the experimental data (black) depending on acid concentration. Values of $PT_i(0)$ are shown as a function of initial sulfuric acid concentration $[H_2SO_4]_0$ (mol L⁻¹). Unfilled shapes indicate $PT_1(0)$ values, and filled shapes indicate $PT_2(0)$ values. Exponential regression curves are shown for $PT_1(0)$ values (solid green line) and $PT_2(0)$ values (dashed green line) for the simulation BZR2.

by $[Fe(phen)_3]^{3+}$ thus poses the question as to how the acidity of the medium might affect the reaction between BrMA and $[Fe(phen)_3]^{3+}$. The pK_a values of malonic acid[69] are 2.9 and 5.7, and one can be fairly certain that bromomalonic acid will be present as a neutral dicarboxylic acid in the pH range of the measurements. Hence, the focus has to be on the $[Fe(phen)_3]^{3+}$ species and its solvation and aggregation. It has been pointed out that, in order for an outer sphere electron transfer to occur, the electron donor must first come in close contact with the electron acceptor and that bulky ligands and coordinated anions may block the approach of the electron donor.[70,71] Investigations into the effects of anions on the rate of electron transfer between substitution-inert transition metal complexes showed both increases[72−75] and decreases[76,77] in the rates of electron transfer reactions as a result of anion addition. These different anion effects can be rationalized by noting that all the increased reaction rates are between two transition metal cations and the decreased reaction rates are between two neutral transition metal complexes or a neutral transition metal complex and a cation. Reaction rates between cations are slow because of electrostatic repulsion, and the formation of ion pairs can decrease electrostatic repulsion and thereby increase reaction rates. On the other hand, aggregation of anions with neutral transition metal complexes can block electron transfer sites and slow electron transfer reaction rates. In our case, we have a cationic transition metal complex reacting with a neutral molecule, and one would expect that this reaction would be slowed by aggregation of anions with the transition metal complex. Any trication will tend to aggregate as much as possible with counteranions to maximize

its electrostatic stabilization. Crystal structures exist of a few $[Fe(phen)_3]^{3+}$ complexes,[78,79] and many more crystal structures are known for $[Fe(phen)_3]^{2+}$ complexes;[80] all of them feature $[Fe(phen)_3]^{u+}$ units which are wholly embedded in shells of counterions. Hydrogensulfate is by far the most abundant anion in the BZ reaction, and one may therefore anticipate the presence of $[Fe(phen)_3(HSO_4)_n(H_2O)_m]^{(3-n)+}$ species ($n = 0-3$). The approach of BrMA necessitates the displacements of solvating water and of aggregating HSO_4^- counterions. Our results suggest that protonation of HSO_4^- by H_3O^+ is required so that BrMA can replace a *neutral* H_2SO_4 molecule in the solvation shell of the oxidant. The insertion of BrMA into the solvent shell of the $[Fe(phen)_3]^{3+}$ species is one requirement, and the second-order dependence on the proton concentration further suggests that BrMA is oxidized by a doubly charged $[Fe(phen)_3(HSO_4)_1(L)_k]^{2+}$ species, where L stands for any neutral molecule (i.e., H_2O, H_2SO_4, BrMA). In other words, the electrostatic stabilization of the oxidant by the aggregated anions reduces the oxidation potential of the Fe^{3+}-system[76] and causes a kinetic barrier as it prevents the approach of BrMA. Vice versa, the removal of these anions by protonation creates a better oxidant and facilitates the approach of the reductant BrMA.
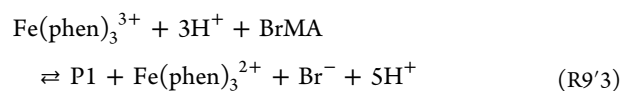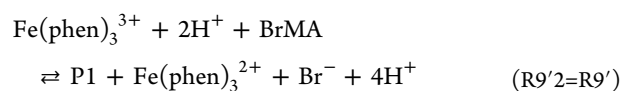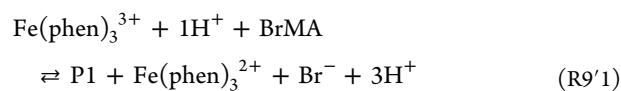
CONCLUSIONS

The acidity dependence of the iron-catalyzed bromate-malonic acid Belousov−Zhabotinsky reaction was studied in the range $0.36\ M < [H_2SO_4]_0 < 1.20\ M$ for at least 2500 s with all other initial conditions being equal. Mathematical methods for image analysis of the video-recordings were developed to analyze the temporal evolution of the oscillation patterns. The effects were quantified for the initial sulfur acid concentration $[H_2SO_4]_0$ on the temporal evolution of period times PT_i, oxidation times OT, and reduction times RT as well as of the intensity variations. Linear regression for the reaction parameters $PT_{min}(t)$, $PT_{max}(t)$, $OT(t)$, and $RT(t)$ shows only very small changes over the measured reaction times, and each reaction is well-characterized by the intercepts $PT_i(0)$, $OT(0)$, and $RT(0)$. The results show that the period times PT_i decrease exponentially with increasing acidity. Furthermore, the results show similar oxidation times over the acidity range while the decrease of the period times with increasing acidity primarily reflects the decrease of the reduction times RT with increasing acidity.

To understand the effect of acidity on the kinetics of the BZ reaction, we simulated the BZ reactions with the dynamical method using all of the reactions of the core reaction mechanism listed in Table 1 and the experimental initial concentrations of Table 2 (the BZR1 system). The simulations of the BZR1 system failed to match the measurements even in a qualitative fashion. Instead, we found that agreement between the experiments and the simulations can only be achieved with the inclusion of proton-catalysis of the outer shell electron transfer reaction between the oxidized [Fe-(phen)_3]^{3+} species and bromomalonic acid in reaction R9. The simulation of reaction R9 with a second-order dependence on $[H^+]$ (the BZR2 system) results in compelling agreement with experiment over the entire range of acidities measured.

The suggested proton-dependence of the oxidation of BrMA by $[Fe(phen)_3]^{3+}$ informs about the species involved in the outer sphere electron transfer reaction. The trication species $[Fe(phen)_3]^{3+}$ will be stabilized by ion pairing and solvation and one may anticipate the presence of $[Fe(phen)_3-$

$(HSO_4)_n(H_2O)_m]^{(3-n)+}$ species ($n = 0-3$). The approach of BrMA necessitates the displacements of solvating water and of aggregating HSO_4^- counterions. Our results suggest that protonation of HSO_4^- by H_3O^+ is required so that BrMA can replace a *neutral* H_2SO_4 molecule in the solvation shell of the oxidant and the second-order dependence on the proton concentration further suggests that BrMA is oxidized by a doubly charged $[Fe(phen)_3(HSO_4)_1(L)_k]^{2+}$ species, where L stands for any neutral molecule (i.e., H_2O, H_2SO_4, BrMA). In other words, the electrostatic stabilization of the oxidant by the aggregated anions reduces the oxidation potential of the Fe^{3+}-system and causes a kinetic barrier as it prevents the approach of BrMA.

Considering the complexity of the system and the uncertainties in the many reaction rate constants in the BZR2 system (Table 1 with reaction R9′), we were somewhat surprised to find this high level of agreement by (just) the replacement of reaction R9 by reaction R9′. In fact, this high level of agreement presents a powerful corroboration of the core reaction mechanism of the BrMA-rich BZ reaction and the replacement of reaction R9 by reaction R9′ extends the validity of this core reaction mechanism to acidities above and below the typical acidity of BZ reactions ($[H^+] \approx 1\ M$). There are several possibilities to optimize the reaction system, and some will have higher priority than others. Our results obviously imply that one ought to include an analogous $[H^+]$ dependence on R10, the oxidation of malonic acid by the oxidized catalyst. For the present case of BrMA-rich BZ reactions, the reduction of the $[Fe(phen)_3]^{3+}$ species is accomplished essentially in full by BrMA, and hence, R10 or any of its proton-catalyzed variants are not competitive. It will be a high priority to improve the kinetic rate equations of all possible reactions between $[Fe(phen)_3]^{3+}$ species and BrMA.

$$Fe(phen)_3^{3+} + 1H^+ + BrMA$$
$$\rightleftharpoons P1 + Fe(phen)_3^{2+} + Br^- + 3H^+ \qquad (R9'1)$$

$$Fe(phen)_3^{3+} + 2H^+ + BrMA$$
$$\rightleftharpoons P1 + Fe(phen)_3^{2+} + Br^- + 4H^+ \qquad (R9'2=R9')$$

$$Fe(phen)_3^{3+} + 3H^+ + BrMA$$
$$\rightleftharpoons P1 + Fe(phen)_3^{2+} + Br^- + 5H^+ \qquad (R9'3)$$

Our results suggest that the *second*-order dependence on $[H^+]$ in the modified reaction R9′ is key to matching experiments and simulations. However, one cannot exclude parallel reactions with *first*-order and/or *third*-order $[H^+]$ dependencies in the modified versions of reaction R9. Of course, the reaction rate constants differ for the reactions reaction R9′p and the good agreement obtained here suggests that the commonly employed k_{9f} value is a close approximation of the reaction rate constant $k_{9'f}$ of reaction R9′. The inclusion of all processes reaction R9′p) should lead to a better fit with the experimental period and oxidation times and the contribution of reaction R9′3 promises a higher curvature of $PT_i(0) = f([H_2SO_4]_0)$.

ASSOCIATED CONTENT

ⓈSupporting Information

The Supporting Information is available free of charge on the ACS Publications website at DOI: 10.1021/acs.jpca.8b05015.

Details regarding acidity effects, figure versions for all reactions, and simulated OT and RT data (PDF)

■ AUTHOR INFORMATION

Corresponding Authors

*E-mail: glaserr@missouri.edu.

*E-mail: chiconec@missouri.edu.

ORCID

Rainer Glaser: 0000-0003-3673-3858

Carmen Chicone: 0000-0002-8692-1411

Notes

The authors declare no competing financial interest.

■ REFERENCES

(1) Zhabotinsky, A. M.; Zaikin, A. N. Concentration Wave Propagations in Two-Dimensional Liquid-Phase Self-Oscillating System. *Nature* **1970**, *225*, 535−537.

(2) Zhabotinskii, A. M. The Early Period of Systematic Studies of Oscillations and Waves in Chemical Systems. In *Oscillations and Traveling Waves in Chemical Systems*; Field, R. J., Burger, M., Eds.; Wiley: New York, 1985; pp 1−6.

(3) Belousov, B. P. A Periodic Reaction and Its Mechanism. In *Oscillations and Traveling Waves in Chemical Systems*; Field, R. J., Burger, M., Eds.; Wiley: New York, 1985; pp 605−660.

(4) Sobel, S. G.; Hastings, H. M.; Field, R. J. Oxidation State of BZ Reaction Mixtures. *J. Phys. Chem. A* **2006**, *110*, 5−7.

(5) Delgado, J.; Zhang, Y.; Xu, B.; Epstein, I. R. Terpyridine- and Bipyridine-Based Ruthenium Complexes as Catalysts for the Belousov-Zhabotinsky Reaction. *J. Phys. Chem. A* **2011**, *115*, 2208−2215.

(6) Toth, R.; Taylor, A. F. The Tris(2,2'-bipyridyl)ruthenium-Catalyzed Belousov-Zhabotinsky Reaction. *Prog. React. Kinet. Mech.* **2006**, *31*, 59−115.

(7) Ueki, T.; Watanabe, M.; Yoshida, R. Belousov−Zhabotinsky Reaction in Protic Ionic Liquids. *Angew. Chem., Int. Ed.* **2012**, *51*, 11991−11994.

(8) Shakhashiri, B. In *Chemical Demonstrations*; University of Wisconsin Press: Madison, WI, 1985; Vol. 2, Chapter 7.6, pp 273−275.

(9) Li, H. Experimental Studies on the Complex Oscillatory Behavior in Gallic Acid-BrO$_3^-$-Mn^{2+}-H$_2$SO$_4$ System. *Ind. J. Chem. A* **1997**, *36*, 823−828.

(10) Lin, H. P.; Jwo, J. J. Kinetic Study of the Belousov-Zhabotinskii Reaction with Phenylmalonic Acid. *J. Phys. Chem.* **1995**, *99*, 6897−6902.

(11) Doona, C. J.; Kustin, K.; Orban, M.; Epstein, I. R. Systematic Design of Chemical Oscillators. 74. Newly Designed Permanganate-Reductant Chemical Oscillators. *J. Am. Chem. Soc.* **1991**, *113*, 7484−7489.

(12) Hu, G.; Chen, L.; Zhang, J.; Chen, P.; Wang, W.; Song, J.; Qiu, L.; Song, J.; Hu, L. Determination of Alizarin Red S Using a Novel B-Z Oscillation System Catalyzed by a Tetraazamacrocyclic Complex. *Cent. Eur. J. Chem.* **2009**, *7*, 291−297.

(13) Körös, E.; Orbán, M. Uncatalyzed Oscillatory Chemical Reactions. *Nature* **1978**, *273*, 371−372.

(14) Orbán, M.; Körös, E. Chemical Oscillations during the Uncatalyzed Reaction of Aromatic Compounds with Bromate. 1. Search for Chemical Oscillators. *J. Phys. Chem.* **1978**, *82*, 1672−1674.

(15) Orbán, M.; Körös, E.; Noyes, R. M. Chemical Oscillations during the Uncatalyzed Reaction of Aromatic Compounds with Bromate. 2. A Plausible Skeletal Mechanism. *J. Phys. Chem.* **1979**, *83*, 3056−3057.

(16) Liu, J.; Scott, S. K. Hysteresis and Complex Oscillations of the Uncatalysed Belousov-Zhabotinskii Reaction in a Stirred Flow Reactor. *J. Chem. Soc., Faraday Trans.* **1991**, *87*, 2135−2140.

(17) Liu, J.; Scott, S. K. Mechanism for the Uncatalysed Belousov-Zhabotinskii Reaction in Open Systems. *J. Chem. Soc., Faraday Trans.* **1992**, *88*, 909−916.

(18) Liu, J.; Scott, S. K. Reduced Models for the Uncatalyzed Belousov-Zhabotinskii Reaction. *J. Phys. Chem.* **1992**, *96*, 9870−9875.

(19) Ren, L.; She, W.; Gao, Q.; Pan, C.; Ji, C.; Epstein, I. R. Retrograde and Direct Wave Locomotion in a Photosensitive Self-Oscillating Gel. *Angew. Chem., Int. Ed.* **2016**, *55*, 14301−14305.

(20) Cherkashin, A. A.; Vanag, V. K. Self-Organization Induced by Self-Assembly in Microheterogeneous Reaction-Diffusion System. *J. Phys. Chem. B* **2017**, *121*, 2127−2131.

(21) Ito, K.; Ezaki, T.; Suzuki, S.; Kobayashi, R.; Hara, Y.; Nakata, S. Synchronization of Two Self-Oscillating Gels Based on Chemo-Mechanical Coupling. *J. Phys. Chem. B* **2016**, *120*, 2977−2983.

(22) Torbensen, K.; Rossi, F.; Pantani, O. L.; Ristori, S.; Abou-Hassan, A. Interaction of the Belousov-Zhabotinsky Reaction with Phospholipid Engineered Membranes. *J. Phys. Chem. B* **2015**, *119*, 10224−10230.

(23) Voorsluijs, V.; Kevrekidis, I. G.; De Decker, Y. Nonlinear Behavior and Fluction-Induced Dynamics in the Photonsensitive Belousov-Zhabotinsky Reaction. *Phys. Chem. Chem. Phys.* **2017**, *19*, 22528−22537.

(24) Torbensen, K.; Ristori, S.; Rossi, F.; Abou-Hassan, A. Tuning the Chemical Communication of Oscillating Microdroplets by Means of Membrane Composition. *J. Phys. Chem. C* **2017**, *121*, 13256−13264.

(25) Smelov, P. S.; Vanag, V. K. Experimental Investigation of a Unidirectional Network of Four Chemical Oscillators Pulse-Coupled through an Inhibitor. *Russ. J. Phys. Chem. A* **2017**, *91*, 1015−1020.

(26) Muñuzuri, A. P.; Pérez-Mercader, J. Noise-Induced and Control of Collective Behaviior in a Population of Coupled Chemical Oscillators. *J. Phys. Chem. A* **2017**, *121*, 1855−1860.

(27) Hastings, H. M.; Field, R. J.; Sobel, S. G.; Guralnick, D. Oreganotor Scaling by the Showalter-Noyes Limit. *J. Phys. Chem. A* **2016**, *120*, 8006−8010.

(28) Simakov, D. S. A.; Pérez-Mercader, J. Effect of Noise Correlation on Noise Induced Oscilaltion Frequency in the Photosensitive Belousov-Zhabotinsky reaction in a Continuous Stirred Tank Reactor. *J. Phys. Chem. A* **2013**, *117*, 13999−14005.

(29) Field, R. J.; Köros, E.; Noyes, R. M. Oscillations in Chemical Systems. II. Thorough Analysis of Temporal Oscillation in the Bromate-Cerium-Malonic Acid System. *J. Am. Chem. Soc.* **1972**, *94*, 8649−8664.

(30) Field, R. J.; Försterling, H. D. On the Oxybromine Chemistry Rate Constants with Cerium Ions in the Field-Körös-Noyes Mechanism of the Belousov-Zhabotinskii Reaction: The Equilibrium HBrO$_2$ + BrO$_3^-$ ↔ 2BrO$_2$● + H$_2$O. *J. Phys. Chem.* **1986**, *90*, 5400−5407.

(31) Försterling, H. D.; Varga, M. HBrO$_2$/Ce^{4+} Reaction and HBrO$_2$ Disproportionation Measured in Sulfuric Acid Solution at Different Acidities. *J. Phys. Chem.* **1993**, *97*, 7932−7938.

(32) Ágreda B, J. A.; Field, R. J. Activation Energy for the Disproportionation of HBrO$_2$ and Estimated Heats of Formation of HBrO$_2$ and BrO$_2$. *J. Phys. Chem. A* **2006**, *110*, 7867−7873.

(33) Hegedüs, L.; Wittmann, M.; Nosztziczius, Z.; Yan, S.; Sirimungkala, A.; Försterling, H. D.; Field, R. J. HPLC Analysis of Complete BZ Systems. Evolution of the Chemical Composition in Cerium and Ferroin Catalysed Batch Oscillators: Experiments and Model Calculations. *Faraday Discuss.* **2002**, *120*, 21−38.

(34) Chou, Y. C.; Lin, H. P.; Sun, S. S.; Jwo, J. J. Kinetic Study of the Ferriin Oxidation of Malonic Acid and Its Derivatives. Implication in

the Belousov-Zhabotinsky Reaction. *J. Phys. Chem.* **1993**, *97*, 8450−8457.

(35) Szalai, I.; Oslonovitch, J.; Försterling, H. D. Oscillations in the Bromomalonic Acid/Bromate System Catalyzed by [Ru(phen)$_3$]$^{2+}$. *J. Phys. Chem. A* **2000**, *104*, 1495−1498.

(36) Rovinsky, A. B. Bromomalonic Acid Oxidation by the Fe(phen)$_3$$^{3+}$ Ion as a Part of the Belousov-Zhabotinsky Oscillatory Process. *J. Phys. Chem.* **1984**, *88*, 4−5.

(37) Sirimungkala, A.; Försterling, H. D.; Dlask, V.; Field, R. J. Bromination Reactions Important in the Mechanism of the Belousov-Zhabotinsky System. *J. Phys. Chem. A* **1999**, *103*, 1038−1043.

(38) Smoes, M. L. Period of Homogeneous Oscillations in the Ferroin-Catalyzed Zhabotinskii System. *J. Chem. Phys.* **1979**, *71*, 4669−4679.

(39) Misra, G. P.; Washington, R. P.; Pojman, J. A. New Experimental and Computational Results on the Radical-Controlled Oscillating Belousov-Zhabotinsky Reaction. *J. Phys. Chem. A* **1998**, *102*, 612−619.

(40) Hsu, W. T.; Jwo, J. J. Kinetic Study of the Ce(III)-, Mn(II)- or Fe(phen)$_3$$^{2+}$-Catalyzed Belousov-Zhabotinsky Reaction with Ethyl Hydrogen Malonate. *Int. J. Chem. Kinet.* **2000**, *32*, 52−61.

(41) Skrabal, A.; Weberitsch, S. R. Zur Kenntnis der Halogensauer-stoffverbindungen. IX. Die Kinetik der Bromat-Bromidreaktion. *Monatsh. Chem.* **1915**, *36*, 211−235.

(42) Sullivan, J. C.; Thompson, R. C. Kinetic Study of the Ce(IV)-Bromous Acid Reaction in Acid Sulfate Solution. Implications for the Belousov-Zhabotinsky Oscillating Reaction. *Inorg. Chem.* **1979**, *18*, 2375−2379.

(43) Noszticzius, Z.; Noszticzius, E.; Schelly, Z. A. On the Use of Ion-Selective Electrodes for Monitoring Oscillating Reactions. 2. Potential Response of Bromide- and Iodide-Selective Electrodes in Slow Corrosive Processes. Disproportionation of Bromous and Iodous Acids. A Lotka-Volterra Model for the Halate Driven Oscillators. *J. Phys. Chem.* **1983**, *87*, 510−524.

(44) Faria, R. d. B.; Epstein, R. I.; Kustin, K. Kinetics of Disproportionation and pK_a of Bromous Acid. *J. Phys. Chem.* **1994**, *98*, 1363−1367.

(45) Glaser, R.; Jost, M. Disproportionation of Bromous Acid HOBrO by direct O-Transfer and via Anhydrides O(BrO)$_2$ and BrO-BrO$_2$. An Ab Initio Study of the Mechanism of a Key Step of the Belousov-Zhabotinsky Oscillating Reaction. *J. Phys. Chem. A* **2012**, *116*, 8352−8365.

(46) Shakashiri, B. Z. Cerium-Catalyzed Bromate-Malonic Acid Reaction. In *Chemical Demonstrations*; The University of Wisconsin Press: Madison, WI; Vol. 2, p 257.

(47) Aoao Photo. http://www.aoaophoto.com (accessed 05/20/2018).

(48) Aoao Video to Picture Converter. https://www.aoaophoto.com/video-to-picture-converter/video-to-picture.htm (accessed 05/20/2018).

(49) *Mathematica*, Version 10.2; Wolfram Research, Inc.: Champaign, IL, 2015. http://www.wolfram.com/mathematica/ (accessed 05/20/2018).

(50) Aoao Video to Picture Converter. https://www.aoaophoto.com/video-to-picture-converter/video-to-picture.htm (accessed 05/20/2018).

(51) Maleki, N.; Safavi, A.; Sedaghatpour, F. Single-Step Calibration, Prediction and Real Samples Data Acquisition for Artificial Neural Network Using a CCD Camera. *Talanta* **2004**, *64*, 830−835.

(52) Firdaus, M. L.; Alwi, W.; Trinoveldi, F.; Rahayu, I.; Rahmidar, L.; Warsito, K. Determination of Chromium and Iron Using Digital Image-Based Colorimetry. *Procedia Environ. Sci.* **2014**, *20*, 298−304.

(53) dos Santos Benedetti, L. P.; dos Santos, V. B.; Silva, T. A.; Filho, E. B.; Martins, V. L.; Fatibello-Filho, O. A. Digital Image-Based Method Employing a Spot-Test for Quantification of Ethanol in Drinks. *Anal. Methods* **2015**, *7*, 4138−4144.

(54) Kohl, S. K.; Landmark, J. D.; Stickle, D. F. Demonstration of Absorbance Using Digital Color Image Analysis and Colored Solutions. *J. Chem. Educ.* **2006**, *83*, 644−646.

(55) Huang, W. E.; Smith, C. C.; Lerner, D. N.; Thornton, S. F.; Oram, A. Physical Modelling of Solute Transport in Porous Media: Evaluation of an Imaging Technique using UV excited Fluorescent Dye. *Water Res.* **2002**, *36*, 1843−1853.

(56) Li, W.; Zhang, R.; Wang, H.; Jiang, W.; Wang, L.; Li, H.; Wu, T.; Du, Y. Digital Image Colorimetry Coupled with a Multichannel Membrane Filtration-Enrichment Technique to Detect Low Concentration Dyes. *Anal. Methods* **2016**, *8*, 2887−2894.

(57) Lopez-Molinero, A.; Cubero, V. T.; Irigoyen, R. D.; Piazuelo, D. S. Feasibility of Digital Image Colorimetry-Application for Water Calcium Hardness Determination. *Talanta* **2013**, *103*, 236−244.

(58) da Nobrega Gaiao, E.; Martins, V. L.; da Silva Lyra, W.; de Almeida, L. F.; da Silva, E. C.; Araújo, M. C. U. Digital Image-Based Titrations. *Anal. Chim. Acta* **2006**, *570*, 283−290.

(59) Tôrres, A. R.; da Silva Lyra, W.; de Andrade, S. I. E.; Andrade, R. A. N.; da Silva, E. C.; Araújo, M. C. U.; da Nóbrega Gaião, E. A. Digital Image-Based Method for Determining of Total Acidity in Red Wines Using Acid−Base Titration without Indicator. *Talanta* **2011**, *84*, 601−606.

(60) Dong, W.; Selvadurai, A. P. S.; Suits, L. D.; Sheahan, T. C. Image Processing Technique for Determining the Concentration of a Chemical in a Fluid-Saturated Porous Medium. *Geotech. Test. J.* **2006**, *29*, 100024.

(61) Hsieh, K. T.; Urban, P. L. Spectral Imaging of Chemical Reactions Using a Computer Display and a Digital Camera. *RSC Adv.* **2014**, *4*, 31094−31100.

(62) Glaser, R. E.; Delarosa, M. A.; Salau, A. O.; Chicone, C. Dynamical Approach to Multi-Equilibria Problems for Mixtures of Acids and their Conjugate Bases. *J. Chem. Educ.* **2014**, *91*, 1009−1016.

(63) Zars, E.; Schell, J.; Delarosa, M. A.; Chicone, C.; Glaser, R. E. Dynamical Approach to Multi-Equilibria Problems Considering the Debye-Hückel Theory of Electrolyte Solutions: Concentration Quotients as a Function of Ionic Strength. *J. Solution Chem.* **2017**, *46*, 643.

(64) Schell, J.; Zars, E.; Chicone, C.; Glaser, R. E. Simultaneous Determination of All Species Concentrations in Multi-Equilibria for Aqueous Solutions of Dihydrogen Phosphate Considering Debye-Hückel Theory. *J. Chem. Eng. Data* **2018**, *63*, 2151−2161.

(65) Horn, F.; Jackson, R. General Mass Action Kinetics. *Arch. Ration. Mech. Anal.* **1972**, *47*, 81−116.

(66) Wolfram Mathematica 9.0 Documentation Center, Wolfram Research Inc. http://reference.wolfram.com/language/ref/NDSolve.html (accessed 05/20/2018).

(67) Smith, W. R.; Missen, R. W. Using Mathematica and Maple to Obtain Chemical Equations. *J. Chem. Educ.* **1997**, *74*, 1369−1371.

(68) Corraine, M. S.; Lai, C. K.; Zhen, Y.; Churchill, M. R.; Buttrey, L. A.; Ziller, J. W.; Atwood, J. D. Kinetics of the Reduction of Co(*o*-phen)$_3$$^{3+}$ by the Metal Carbonyl Anions Re(CO)$_5$$^-$, Mn(CO)$_4L^-$ (L = CO, PEt$_3$, PBu$_3$, PPh$_3$), Co(CO)$_4$$^-$, CpMo(CO)$_3$$^-$, and CpFe(CO)$_2$$^-$ (Cp = η^5-C$_5$H$_5$, *o*-phen = *o*-Phenanthroline). Structural Determinations of [PPN$^+$][Mn(CO)$_5$$^-$] and [PPN$^+$][Mn(CO)$_4$(PEt$_3$)$^-$]●THF. *Organometallics* **1992**, *11*, 35−40.

(69) *CRC Handbook of Chemistry and Physics*, 95th ed.; Haynes, W. M., Ed.; CRC Press: Boca Raton, FL, 2014.

(70) Ford-Smith, M. H.; Sutin, N. The Kinetics of the Reactions of Substituted 1,10-Phenanthroline, 2,2'-Dipyridine and 2,2',2''-Tripyridene Complexes of Iron(III) with Iron(II) Ions. *J. Am. Chem. Soc.* **1961**, *83*, 1830−1834.

(71) Dickens, J. E.; Basolo, F.; Neumann, H. M. Mechanism of Racemization of Complex Ions. III. Effect of Added Ions upon the Rates of Dissociation of Tris-(1,10-phenanthroline)-iron(II) and Tris-(1,10-phenanthroline)-iron(III) and upon the Rate of Racemization of Tris-(1,10-phenanthroline)-iron(III). *J. Am. Chem. Soc.* **1957**, *79*, 1286−1290.

(72) Stalnaker, N. D.; Solenberger, J. C.; Wahl, A. C. Electron-Transfer between Iron, Ruthenium, and Osmium Complexes Containing 2,2'-Bipyridyl, 1,10-Phenanthroline, or Their Derivatives. Effects of Electrolytes on Rates. *J. Phys. Chem.* **1977**, *81*, 601−604.

(73) Schmid, R.; Kirchner, K.; Dickert, F. L. Redox Kinetics of Metal Complexes in Nonaqueous Solutions: Reductions of Tris(1,10-phenanthroline)- and Tris(2,2'-bipyridine)iron(III) by Hexakis(*N,N*-dimethylformamide)iron(II) in Acetonitrile: Role of First Coordination Sphere. *Inorg. Chem.* **1988**, *27*, 1530−1536.

(74) Wangila, G. W.; Jordan, R. B. Kinetic Studies of Tris(2,2'-bipyridine)iron(III) Perchlorate with Cobaloxime, [Co-(dmgBF$_2$)$_2$(H$_2$O)$_2$]. *Inorg. Chim. Acta* **2005**, *358*, 2804−2812.

(75) Du, G.; Espenson, J. H. Kinetics of the Reaction of Chromium(VI) with Tris(1,10-phenanthroline)iron(II) Ions in Acidic Solutions. Anion and Medium Effects: Perchlorate versus Triflate. *Inorg. Chem.* **2006**, *45*, 1053−1058.

(76) Borchardt, D.; Wherland, S. Solvent, Temperature, and Electrolyte Studies on the Electron-Transfer Reaction between Ferrocene and a Cobalt Clathrochelate. *Inorg. Chem.* **1984**, *23*, 2537−2542.

(77) Borchardt, D.; Wherland, S. Electron-Transfer Studies on a Series of Cobalt Clathrochelates in Acetonitrile. *Inorg. Chem.* **1986**, *25*, 901−905.

(78) Baker, L.; Engelhardt, L. M.; Figgis, B. N.; White, A. H. Crystal Structure, Electron Spin Resonance, and Magnetism of Tris-(*o*-phenanthroline)iron(III) Percholorate Hydrate. *J. Chem. Soc., Dalton Trans.* **1975**, 530−534.

(79) Odoko, M.; Okabe, N. Tris(1,10-phenanthroline−$\kappa^2 N,N'$)iron-(III) Trinitrate Monohydrate. *Acta Crystallogr., Sect. E: Struct. Rep. Online* **2004**, *E60*, m1822−m1824.

(80) Teramoto, K.; Kawasaki, T.; Nishide, T.; Ikeda, Y. Crystal Structure of Tris(1,10-phenanthroline-$\kappa^2 N,N'$)iron(II) Bis[bis-(trifluoromethylsulfonyl)imide] Monohydrate. *Acta Crystallogr.* **2015**, *E71*, m8−m9.